- A Study of the Dependence between Soil Moisture and
- 2 Precipitation in different Ecoregions of the Northern
- 3 Hemisphere

4

5 Shouye Xue^a and Guocan Wu ^{a*}

6

- ^a State Key Laboratory of Earth Surface Processes and Disaster Risk Reduction,
- 8 Faculty of Geographical Science, Beijing Normal University, Beijing, 100875, China

9

*Corresponding author: Guocan Wu, gcwu@bnu.edu.cn

11

Abstract

13

14

15

16

17

18

19

20

21

22

23

24

25

26

27

28

29

30

31

32

33

34

35

36

37

38

39

40

Soil moisture plays a critical role in the land-atmosphere coupling system. It is replenished by precipitation and transported back to the atmosphere through land surface evaporation and vegetation transpiration. Soil moisture is, therefore, influenced by both precipitation and evapotranspiration, with spatial heterogeneities and seasonal variations across different ecological zones. Recently, negative correlations between soil moisture and precipitation have been observed in Northern Hemisphere ecosystems. However, the driving mechanisms of these negative correlations, especially how soil moisture is influenced by precipitation and evapotranspiration, still remain unclear. This study analyzes the dependence between soil moisture and precipitation in different ecoregions to explore the driving mechanisms and regional patterns. The joint distributions of precipitation and soil moisture were analyzed at monthly and annual scales, using soil moisture and precipitation data from ERA5-Land and Global Precipitation Climatology Project, respectively. The nonlinear negative dependencies reached to 19.2%, 0.7%, and 2.3% at monthly scale, while were 3.0%, 4.0%, and 8.6% at annual scale, respectively, for the three soil layers. These negative dependencies were shown to be most prominent in temperate grasslands, savannas, shrublands, deserts, xeric shrublands, and tundra regions, where driven by the land surface temperature and by the air temperaturegross primary production relationship at the monthly scale based on Ridge regression models and Bayesian models. Additionally, the negative dependence is also linked to freeze-thaw cycles, precipitation seasonality, and temperature fluctuations, which lead to asynchronous changes between soil moisture and precipitation at the seasonal scale. At the annual scale, the negative dependence was associated with long-term changes in precipitation and temperature that affect vegetation and surface properties, by altering soil water capacity. These findings enhance the understanding of landatmosphere interactions providing a valuable basis for future research on drought, hydrometeorology, and ecological conservation.

41 Keywords: climate change, precipitation, soil moisture, ecoregions

1. Introduction

42

43

44

45

46

47

48

49

50

51

52

53

54

55

56

57

58

59

60

61

62

63

64

65

66

67

68

69

70

Soil moisture is a critical source of water for vegetation growth, replenished by precipitation and groundwater, and returned to the atmosphere through evapotranspiration. It plays a key role in weather conditions, vegetation dynamics, and groundwater storage (Li et al., 2022; Qiao et al., 2023; Vereecken et al., 2008; Zhou et al., 2021), with significant implications for the global climate. Surface soil moisture regulates the distribution of available energy at the land surface and exchanges energy with the near-surface atmosphere through sensible and latent heat fluxes, thereby controlling the surface energy balance (Haghighi et al., 2018; McColl et al., 2017). In contrast, deep soil moisture is more directly influenced by vegetation growth, particularly by the development of plant roots, which play a crucial role in the vertical infiltration of precipitation into deeper soil layers (Szutu and Papuga, 2019; Xiao et al., 2024; Xue and Wu, 2024). Precipitation variability, which refers to the amplitude of precipitation fluctuations over different times, influences soil moisture and thereby land surface coupling (Koster et al., 2009; Taylor et al., 2012). Precipitation patterns are reported to have undergone significant changes in recent decades (Lv et al., 2023; Mao et al., 2022; Wu et al., 2021), mainly manifested as anthropogenic amplification of precipitation variability (Zhang et al., 2024). The increase in the frequency of extreme precipitation events (Myhre et al., 2019; Wang et al., 2022) and decrease in the frequency of smaller precipitation events (Ma et al., 2015) amplify soil moisture fluctuations and prolong the moisture stress periods between consecutive precipitation events (Knapp et al., 2008). This can directly affect vegetation growth and soil moisture responses (Feldman et al., 2024; He et al., 2023), particularly through changes in the duration and intensity of soil evaporation and plant transpiration (Gu et al., 2021; Wullschleger and Hanson, 2006). Soil moisture has been shown to be negatively correlated with precipitation in certain regions, based on Pearson correlation analyses (Cook et al., 2006; Yang et al., 2018). The changes in soil moisture at different depths also show notable discrepancies (Shen et al., 2016; Zhu et

al., 2014). Surface soil moisture has been shown to respond to precipitation approximately a month earlier than deeper soil moisture, with a more pronounced positive correlation between precipitation and soil moisture occurring at depths greater than 50 cm (Zhang et al., 2020).

Most current analyses of the relationship between soil moisture and precipitation assume a linear relationship (Sehler et al., 2019; Yang et al., 2018). In reality, the response of soil moisture to precipitation is extremely complex and often nonlinear (Drager et al., 2022). This kind of nonlinear and asymmetric correlation is generally referred to as "dependence". The nonlinear dependence of soil moisture to precipitation is currently not well understood. Moreover, the factors driving this negative dependence between soil moisture and precipitation remain poorly understood due to the complicated land atmosphere coupling processes, particularly in the Northern Hemisphere where different types of vegetation coverage are present. Among the methods used to explore nonlinear relationships, the copula function is one of the most widely applied approaches for modeling the joint distributions of precipitation and soil moisture (Cammalleri et al., 2024). The copula is a stochastic model that can reveal nonlinear and asymmetric dependence structures, which are difficult to capture using traditional linear methods. It provides a flexible framework for modeling joint distributions of multiple variables, allowing for a more precise understanding of the evolving dependence of soil moisture on precipitation than that offered by traditional linear regression and correlation methods.

In terms of the water cycle, soil moisture is replenished by precipitation and groundwater, while also being absorbed by plant roots and lost through evapotranspiration. Therefore, the change of soil moisture is actually simultaneously influenced by precipitation volume, frequency, and evapotranspiration. However, the response of soil moisture to precipitation and evapotranspiration varies across different time scales. The long-term effects of changes in evapotranspiration and precipitation on soil moisture are further shaped by seasonal transitions, with significant differences observed at different soil depths (Szutu and Papuga, 2019).

These differences are influenced by factors such as soil freeze—thaw processes and vegetation community structure. Therefore, the relative contributions of evapotranspiration, precipitation volume, and frequency to soil moisture changes should be quantified at different time scales.

Although previous studies have identified the mechanisms of soil moisture variation across different time scales (shen et al., 2018; Vidana Gamage et al., 2020), the interaction among precipitation, evapotranspiration and soil water under climate change may have changed over different time scales. The dependence of soil moisture to precipitation and its interactions with evapotranspiration under conditions of climate change require further investigation. Accordingly, the ridge regression models for precipitation amount, precipitation frequency, evapotranspiration, and soil moisture can be used to quantify the relative influence of precipitation and evapotranspiration on soil moisture. As an improvement of the least squares estimation method, it can handle the multi-collinearity problems of the covariates, although it is usually biased.

The aim of this study was to explore the nonlinear responses of soil moisture to precipitation at monthly and annual scales from 2000 to 2019, with a focus on the Northern Hemisphere where vegetation coverage is abundant. The joint distribution of precipitation and soil moisture was established to examine differences in soil moisture responses to precipitation and the varying influences of precipitation volume, frequency, and evapotranspiration on soil moisture at monthly and seasonal scales. The gross primary productivity (GPP), land surface temperature (LST), and near-surface air temperature (T_a) were selected as key driving factors in a Bayesian model, since the dependence between precipitation and soil moisture is influenced by factors such as vegetation growth, temperature, and soil properties. The driving factors and regional characteristics of the negative correlation observed between precipitation and soil moisture in certain regions were identified. This study enhances the understanding of complex interactions between key meteorological factors such as precipitation, evapotranspiration, and soil moisture under climate change, and

provides a basis for future land–atmosphere coupling system modeling.

2. Material and Method

2.1 Material

2.1.1 Soil moisture

The soil moisture data used in this study were obtained from the fifth generation of reanalysis from the European Centre for Medium-Range Weather Forecasts (ECMWF), using atmospheric forcing to control the simulated land field variables and provide the land components (ERA5-Land) (Muñoz Sabater, 2019). ERA5-Land provides a consistent description of the evolution of the energy and water cycles over land, and therefore, has been widely used in various land surface applications such as flood or drought forecasting (Joaquín Muñoz-Sabater, 2021). The ERA5-Land soil moisture data are available for four layers, 0 to 7, 7 to 28, 28 to 100, and 100 to 289 cm, at a $0.1^{\circ} \times 0.1^{\circ}$ spatial and hourly temporal resolution from 1950 to present. The soil moisture from the first three soil layers during 2000 to 2019 were used. They were resampled to a $0.25^{\circ} \times 0.25^{\circ}$ spatial resolution and averaged to daily, monthly, and yearly scales to be consistent with other variables in this study.

2.1.2 Precipitation

The Global Precipitation Climatology Project (GPCP) is a global precipitation project that integrates infrared and microwave data from multiple geostationary and polar-orbiting satellites, and corrected by many meteorological station observations (Adler et al., 2003; Huffman and Bolvin, 2013). It is an important component of the Global Energy and Water Cycle Experiment in the World Climate Research Programme. A daily precipitation field with a 1° × 1° resolution since 1996 was generated by integrating the satellite products and then adjusting the daily precipitation by monthly data observed from the ground to make it consistent with the meteorological observations. Daily precipitation was resampled to a 0.25° × 0.25° spatial resolution and then used to calculate the total precipitation volume and

precipitation frequency at the monthly, seasonal, and annual scale from 2000 to 2019.

2.1.3 Covariate variables

156

157

158

2.1.3.1 Gross primary production

- The gross primary production (GPP) dataset was from the Vegetation Optical
- Depth Climate Archive v2, which used microwave remote sensing estimates of
- vegetation optical depth to estimate the GPP at the global scale for the period 1988 to
- 162 2020 (Wild et al., 2022). These GPP data were trained and evaluated against
- 163 FLUXNET in-situ observations and compared with largely independent state-of-the-
- art GPP datasets from the Moderate Resolution Imaging Spectroradiometer (MODIS).
- The Vegetation Optical Depth Climate Archive v2 GPP dataset has a $0.25^{\circ} \times 0.25^{\circ}$
- spatial and half-monthly temporal resolution, covered from 2000 to 2019.

2.1.3.2 Near surface air temperature

- The air temperature data (T_a) were obtained from the Climatic Research Unit
- gridded Time Series (CRU TS), which is one of the most widely used climate datasets
- and is produced by the National Centre for Atmospheric Sciences in the United
- Kingdom. CRU TS v4.07 was derived by the interpolation of monthly climate
- anomalies from extensive networks of weather station observations (Harris et al.,
- 173 2020). It provides monthly land surface data from 1901 to 2020 at a $0.5^{\circ} \times 0.5^{\circ}$
- 174 resolution worldwide. The mean temperatures at the monthly, seasonal, and annual
- scales during 2000 to 2019 were calculated and resampled to a $0.25^{\circ} \times 0.25^{\circ}$ spatial
- 176 resolution.

2.1.3.3 Land surface temperature

- Land surface temperature (LST) data were accessed from the European Space
- 179 Agency Climate Change Initiative (CCI), which is funded by the European Space
- Agency as part of the Agency's CCI Program. It aims to significantly improve current
- satellite LST data records to meet the challenging Global Climate Observing System
- requirements for climate applications and realize the full potential of long-term LST
- data for climate science (Hollmann et al., 2013). These data were the first global LST
- climate data records of over 25 years at a $0.25^{\circ} \times 0.25^{\circ}$ resolution and with an

expected error within 1 K. The LST dataset included ascending and descending orbit data, which were used to calculate the mean value of separate annual and monthly averages during 2000 to 2019.

2.1.3.4 Evapotranspiration

Evapotranspiration data were accessed from the Global Land Evaporation Amsterdam Model (GLEAM) v3.8a, which provides data of the different components of land evapotranspiration, including transpiration, bare-soil evaporation, interception loss, open-water evaporation, and sublimation, in addition to other related variables such as surface and root-zone soil moisture, sensible heat flux, potential evaporation, and evaporative stress conditions (Miralles et al., 2011). The monthly, seasonal, and annual averages during 2000 to 2019 were calculated based on a 0.25° × 0.25° spatial resolution.

2.1.3.5 Terrestrial ecoregions

Data on terrestrial ecoregions around the globe were accessed from the Conservation Biology Institute (Olson et al., 2001). These ecoregions are relatively large units of land containing distinct assemblages of natural communities and species, with boundaries that approximate the original extent of natural communities prior to major land-use changes. The delineations were completed based on hundreds of previous biogeographical studies and were refined and synthesized using existing information in regional workshops over the course of 10 years to assemble the global dataset (Olson et al., 2001). An ecological layer file encompassing 16 major categories was downloaded.

Although the Köppen climate classification provides a standardized framework based on temperature and precipitation, it may perform not well in accounting for critical biophysical factors, particularly for vegetation. Alternatively, the ecoregion divisions integrate both climatic and ecological factors, offering a more comprehensive understanding of the spatial heterogeneity in vegetation types and hydrological processes (Gerken et al., 2019; Olson et al., 2001). This makes it particularly advantageous for studying land—atmosphere interactions, since vegetation

plays a central role in regulating energy and water fluxes. Therefore, this study adopts ecoregion boundaries to better capture the vegetation related variability in precipitation—soil moisture relationship. Since soil moisture dynamics and their feedbacks with precipitation are strongly influenced by vegetation structure, root systems, and edaphic properties, the ecoregions can provide a more mechanistic and spatially relevant framework for our analysis. All of the T_a, LST, GPP, soil moisture, and precipitation datasets were masked by these 16 terrestrial ecoregions (Fig. 1) in a 0.25° grid, and monthly, seasonal, or annual mean values in the regions were calculated separately.

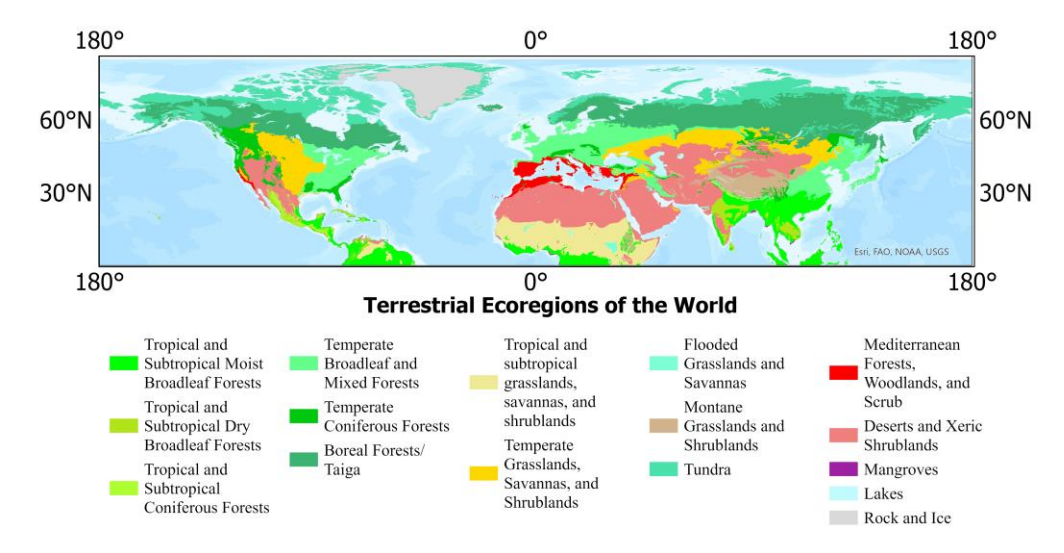


Fig. 1 The 16 Terrestrial Ecoregions of the Northern Hemisphere.

2.2 Method

2.2.1 Joint distribution

In this study, the joint distribution between precipitation and soil moisture from depths of 0 to 7 cm, 7 to 28 cm, and 28 to 100 cm, using the copula function at both the monthly and annual scales was established. A copula function links multivariate distribution functions with their one-dimensional marginal distributions, and is used for the examination of dependencies between multiple variables. It captures nonlinear dependence structures through joint and marginal probabilities of a pair of variables in complex multivariate systems (Nelsen, 2005). In this study, the copula function was

used to explore the nonlinear dependence between precipitation and soil moisture (Equation 1):

236
$$F_{P,SM}(x,y) = C(F_P(x), F_{SM}(y)), \tag{1}$$

where $F_P(x)$ and $F_{SM}(y)$ denote the marginal distribution of precipitation and soil moisture, respectively, and C(u,v) is the copula function linking these two variables. The process for establishing the joint distribution was as follows: (1) The marginal distributions of precipitation and soil moisture were fitted using an automatic optimization function. (2) The most suitable copula function was selected based on the Akaike Information Criterion (AIC) values at the grid level, including Gaussian copula, Student's t copula, Clayton copula, and 37 other copula functions. Different copula functions may be selected for different grid cells. (3) The chosen copula function was then used to compute the corresponding Kendall's tau (τ) , upper tail dependence (λ_U) , and lower tail dependence (λ_L) .

The statistic τ measures the correlation between two variables to determine the presence of a monotonic relationship. λ_U and λ_L represent the likelihood that, when one variable reaches extreme high or low values, the other variable also reaches extreme values. The calculations of τ , λ_U , and λ_L are based on the dependence parameters of the joint distribution of precipitation and soil moisture, and depends on the selected copula function using the AIC method. Taking the Tawn copula function as an example, the calculation of τ , λ_U , and λ_L are based on the following equations.

$$\tau = 1 - \frac{2\delta}{\theta + 1} + \frac{2\delta^2}{2\theta + 1},\tag{2}$$

255
$$\lambda_{U} = (1 - \delta) \cdot (2 - 2^{1/\theta}), \tag{3}$$

256 and

$$\lambda_{L} = \delta \cdot (2 - 2^{1/\theta}), \tag{4}$$

where θ is the dependence parameter of the Tawn copula, and δ represents the asymmetry parameter. For some copula functions, such as Clayton copula, the Kendall's τ values get the priority over the upper and lower tail dependencies in the estimation process. All the calculations were performed using R v4.3.3 with the VineCopula and copula packages, for which detailed calculation methods for τ , λ_U ,

and λ_L for all copulas are provided. To address the potential delayed response of soil moisture to precipitation, lagged correlation analysis was conducted. For each grid cell, the AIC value was calculated to select copula function (Fig. S1), as shown in the supplementary file. Then the Kendall's tau correlation was calculated between precipitation and soil moisture with time lags ranging from 0 to 12 months (Fig. S2). The lag corresponding to the maximum absolute correlation was identified as the optimal lag.

2.2.2 Ridge regression

263

264

265

266

267

268

269

270

271

272

273

274

275

276

277

278

279

280

281

282

283

284

285

287

288

Ridge regression is designed to address collinear data, although it is a biased estimation method. It is an improved least squares estimation used to generate more reliable regression coefficients at the cost of unbiasedness. Ridge regression outperforms the traditional least squares method when fitting ill-conditioned data (McDonald, 2009). Due to the large uncertainty in precipitation and soil moisture data, ridge regression models were applied for three soil layers, and for both monthly and seasonal scales. Spring was defined as from March to May, summer from June to August, autumn from September to November, and winter from December to February of the following year. Precipitation frequency, volume, evapotranspiration were treated as predictor variables, with T_a as a control variable and soil moisture as the response variable.

To clearly differentiate the influence of variables, the regression coefficients for precipitation volume, frequency, and evapotranspiration were normalized using Equation (5) and then assigned to the three primary colors. This approach resulted in a gridded ternary phase diagram.

$$W_i = 1 - \frac{v_i}{\sum_{i=1}^3 v_i},\tag{5}$$

where $v_i(v_1, v_2, v_3)$ represent precipitation frequency, precipitation volume, and evapotranspiration (ET), respectively, and W_i refers to the adjusted weight of v_i .

2.2.3 Bayesian generalized non-linear multivariate multilevel models

289

290

291

292

293

294

295

296

297

298

299

300

301

302

303

304

305

306

307

308

309

310

311

312

315

316

317

The Bayesian generalized non-linear multivariate multilevel model integrates Bayesian inference, generalized linear models, non-linear modeling, multivariate analysis, and hierarchical structures, making it well-suited for complex hierarchical data. It can effectively capture non-linear dependencies among multiple response variables (Browne and Draper, 2006; Bürkner, 2017). The model parameters are treated as random variables with prior distributions under the Bayesian framework. Posterior distributions of the parameters are obtained by combining the likelihood function and prior distributions. The Markov Chain Monte Carlo (MCMC) algorithm is then used to resample from the posterior distribution and estimate the posterior means of the parameters to represent the optimal results. Given the hierarchical and multivariate nature of the data, a multilevel structure and multivariate analysis was introduced to model the mixed effects of variables and to capture the relationships among multiple related response variables. Random effects were also incorporated to account for heterogeneity among individuals and reflect the varying effects of univariate or multivariate mixtures on the response variables, thereby improving the accuracy of estimates.

Since the impact approaches of GPP, LST, and T_a on precipitation (P) and soil moisture (SM) are often unknown, the Gaussian distribution was specified as the prior distribution for these variables in the Bayesian model. To investigate how GPP, LST, and T_a influence the precipitation–soil moisture coupling relationship, both precipitation and soil moisture were treated as response variables. Bayesian non-linear multivariate multilevel models were developed at both the monthly and seasonal scales, with independent models for 16 ecological zones (Equation 6):

Posterior estimates =
$$bf(P \sim T_a + GPP + LST + T_a:GPP + T_a:LST + GPP:LST + T_a:GPP:LST) + T_a:GPP:LST + T_a:GP$$

$$bf(SM \sim T_a + GPP + LST + T_a:GPP + T_a:LST + GPP:LST + T_a:GPP:LST), \qquad (6)$$

where the colon represents multivariate mixed effects of different variables; bf stands for Bayesian formula, used to specify each part of the model for P and SM separately; and the "+" combines P and SM into a multivariate model. The model was

implemented in R 4.3.3 using the brms package, which performs diagnostic checks on the sampling results using indicators such as the Gelman–Rubin diagnostic (Rhat statistic) and the effective sample size (ESS). To ensure stability and convergence, four MCMC chains were used for iterative sampling, with each chain running 4,000 iterations, including 2,000 warm-up iterations. A maximum tree depth of 10 was set. Estimate values of all ecoregions were classified into different clusters using the K-means method in R 4.3.3.

3. Results

3.1 Estimation from the copula function

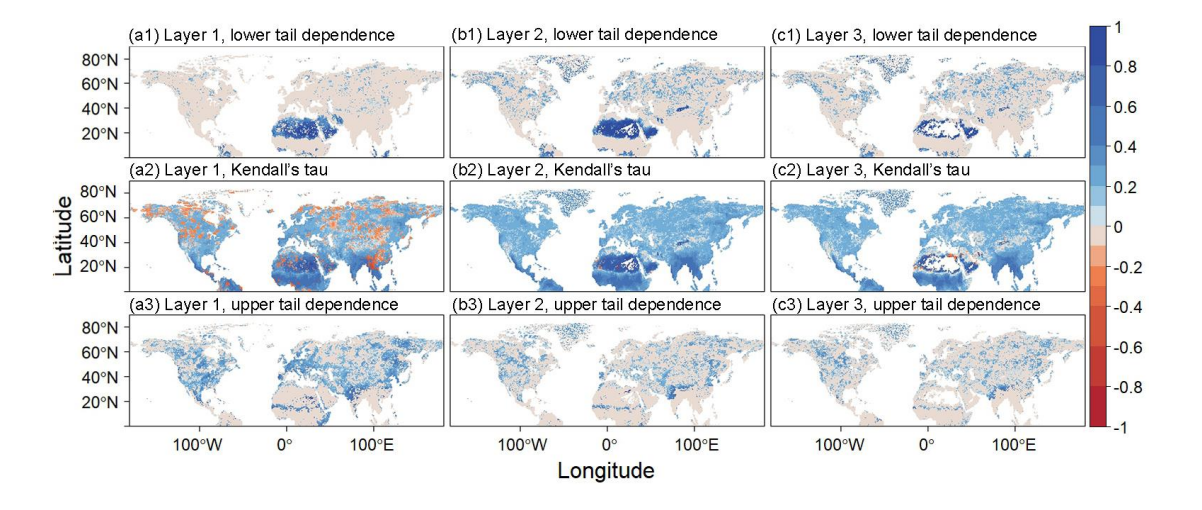


Fig. 2 Spatial distribution of Kendall's tau (τ), the upper tail dependence (λ_U), and the lower tail dependence (λ_L) on the $0.25^\circ \times 0.25^\circ$ grids between monthly precipitation volume and soil moisture during 2000 to 2019. The three columns are for the soil moisture from depths of 0 to 7 cm, 7 to 28 cm, and 28 to 100 cm, respectively.

The copula analysis of monthly average soil moisture and total monthly precipitation volume revealed a clear negative dependence at all three soil depths (Fig. 2(a2, b2, c2)). The percentages of grid cells exhibiting negative dependence at these depths were 19.2%, 0.7%, and 2.3%, respectively. The negative dependence between precipitation and soil moisture is more prevalent in the surface soil layer,

where the grid cells exhibiting are more widespread. In contrast, at the middle and deep soil layers, these negative dependence patterns are primarily confined to the margins of the Sahara desert, the montane grasslands and shrublands, and parts of the deserts and xeric shrublands regions. In the surface layer, the negatively dependent grid patches are more spatially scattered, mainly distributed across the tundra, montane grasslands and shrublands, deserts and xeric shrublands, as well as the tropical and subtropical moist broadleaf forests.

 Regions exhibiting high λ_L values were primarily located in the deserts and xeric Shrublands, as well as in parts of India, where λ_L reached values as high as 0.99 (Fig. 2(a1, b1, c1)). With increasing soil depth, λ_L values gradually increased across the Eurasian continent. Similarly, λ_U exhibited a clear reduction in spatial extent with increasing soil depth, with the majority of these regions located in the temperate broadleaf and mixed forests and the southern margin of the Sahara desert. With increasing soil depth, λ_U values consistently decreased, resulting in a lack of clear correspondence between these regions and specific ecological zones (Fig. 2(a3, b3, c3)). This decreasing trend likely reflects the weakening of extreme precipitation—soil moisture coupling in deeper soil layers, except for arid regions where vegetation is sparse or absent.

From the annual scale copula results (Fig. 3), precipitation and soil moisture generally exhibited positive dependencies across the entire soil profile. However, negative dependencies were observed in regions such as the southern Sahara Desert, Mongolia, and the Elizabeth Islands, reaching 3.0%, 4.0%, and 8.6%, respectively (Fig. 3(a2, b2, c2)). It revealed that the negative correlation was kept between precipitation-soil moisture in long-term scale over arid regions. The negative dependencies in these areas expanded outward, primarily concentrated in the montane grasslands and shrublands region. Both the λ_L and the λ_U displayed scattered, patchy distributions, with average values for each soil layer ranging from 0.4 to 0.6.

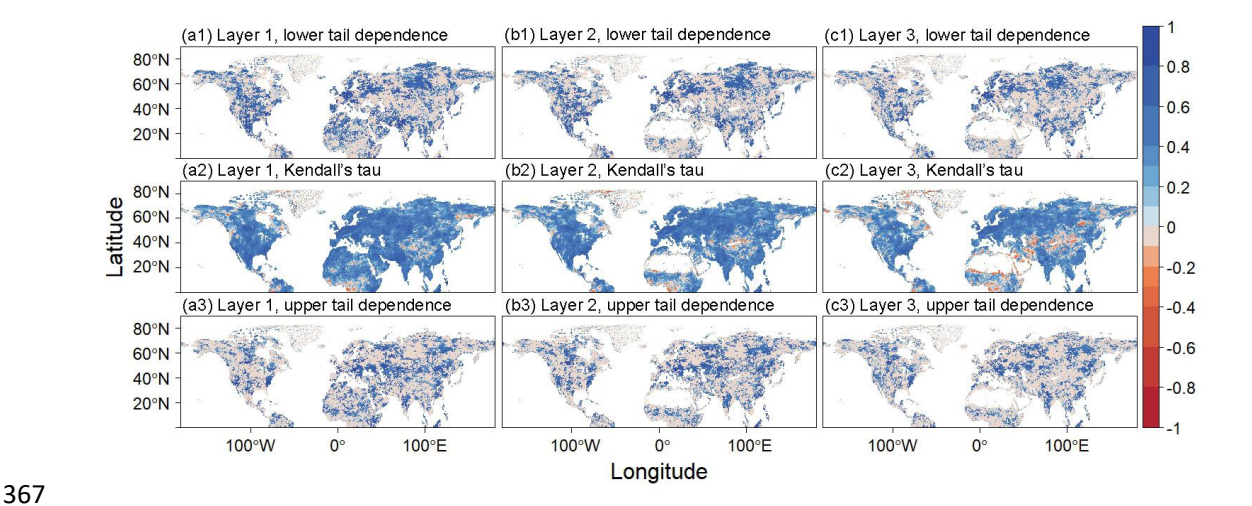


Fig. 3 Spatial distributions of the τ , λ_U , and λ_L on the $0.25^\circ \times 0.25^\circ$ grids between annual precipitation volume and soil moisture during 2000 to 2019. The three columns are for the soil moisture from depths of 0 to 7 cm, 7 to 28 cm, and 28 to 100 cm, respectively.

3.2 Control of soil moisture by precipitation and evapotranspiration

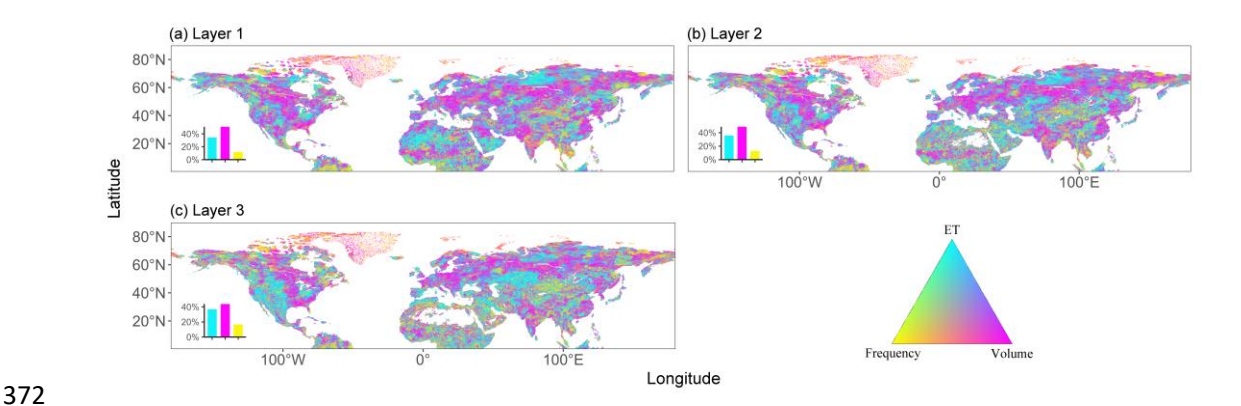


Fig. 4 Ternary map of factors controlling soil moisture, monthly, for the period 2000 to 2019. The bottom-left histogram in the subgraph represents the proportion of grid cells where one variable exerts strong univariate control (with a regression coefficient greater than 75% of the total sum of the three variables), suggesting that soil moisture was predominantly controlled by that specific variable.

On the monthly scale, precipitation exerted the strongest control over soil moisture (Fig. 4), with regions most influenced by precipitation accounting for more than 40% of the variation. These areas were primarily located in the boreal forest/taiga, temperate grasslands, savannas, shrublands, and the eastern part of North

America. In contrast, regions where evapotranspiration predominated were found in Alaska–Northwest Canada, the western United States, the Sahara Desert, and the Middle East. High-latitude regions, especially northern Canada, were primarily influenced by precipitation frequency. Areas where precipitation volume, frequency, and evapotranspiration had similar levels of control were mainly found in Eastern Europe and Russia.

382

383

384

385

386

387

388

389

390

391

392

393

394

395

396

397

398

399

400

401

402

403

404

405

The results from ridge regression revealed more distinct patterns at the seasonal scale compared to the monthly scale (Fig. 5). Soil moisture in spring and summer was mainly controlled by evapotranspiration, which influenced over 40% of grid cells, particularly in the middle soil layers, where it dominated nearly 80%. In contrast, precipitation volume had a greater influence during autumn and winter, particularly in the continental United States, southern Sahara Desert, coastal India, and eastern China. Additionally, as soil depth increased, the influence of evapotranspiration and precipitation frequency gradually intensified. However, in summer, as soil depth increased, the area primarily controlled by precipitation volume expanded (indicated by an increase in the intensity of magenta color in the figures) especially in the eastern United States, Europe, and South Asia. These regions remained strongly influenced by precipitation volume even as evapotranspiration control increased with increasing soil depth during autumn. Northern Russia, Canada, Greenland, and northern Alaska were notably influenced by both precipitation frequency and precipitation volume, with this effect being more pronounced during the non-growing season. In winter, the area controlled by precipitation frequency was larger than that in spring.



Fig. 5 Ternary map of factors controlling soil moisture, seasonally, for the period 2000 to 2019. The bottom-left histogram in the subgraph represents the proportion of the grid cells where one variable exerts strong univariate control (with a regression coefficient greater than 75% of the total sum of the three variables), suggesting that soil moisture was predominantly controlled by that specific variable.

At the annual scale, precipitation amount exerts a dominant influence across all three soil depth layers, accounting for more than 40% of the total area (Fig. 6). The spatial extent of areas dominated by precipitation amount, precipitation frequency, and evapotranspiration remains largely consistent with that observed at the monthly scale. The regions dominated by precipitation frequency are still primarily located in high-latitude areas, particularly in Greenland and the northern parts of Canada, although no distinct ecological zone patterns are observed in these areas. Regions dominated by precipitation amount are mainly distributed across boreal forests, temperate grasslands, savannas and shrublands, temperate broadleaf and mixed forests, as well as tropical and subtropical moist broadleaf forests. In temperate regions, soil moisture is primarily controlled by precipitation amount due to moderate temperatures and limited rainfall, making substantial precipitation is essential for soil moisture replenishment. In contrast, tropical and subtropical regions experience high temperatures and intense evapotranspiration, requiring substantial precipitation to

maintain a water balance.

(a) Layer 1

(b) Layer 2

(c) Layer 3

(c) Layer 3

ET

Frequency Volume

Longitude

Fig. 6 Ternary map of factors controlling soil moisture at annual scale, for the period 2000 to 2019. The bottom-left histogram in the subgraph represents the proportion of grid cells where one variable exerts strong univariate control (with a regression coefficient greater than 75% of the total sum of the three variables), suggesting that soil moisture was predominantly controlled by that specific variable.

3.3 Drivers of negative dependencies between soil moisture and precipitation

For each model in this study, four MCMC chains were used for iterative sampling. The sampling results demonstrated that the chains for both the monthly and annual scales were well-distributed in the parameter space, with no noticeable trends or drifts, indicating convergence to the target posterior distribution. The convergence was considered satisfactory, with all models yielding a Rhat value below 1.05 (Figs. S3, S4).

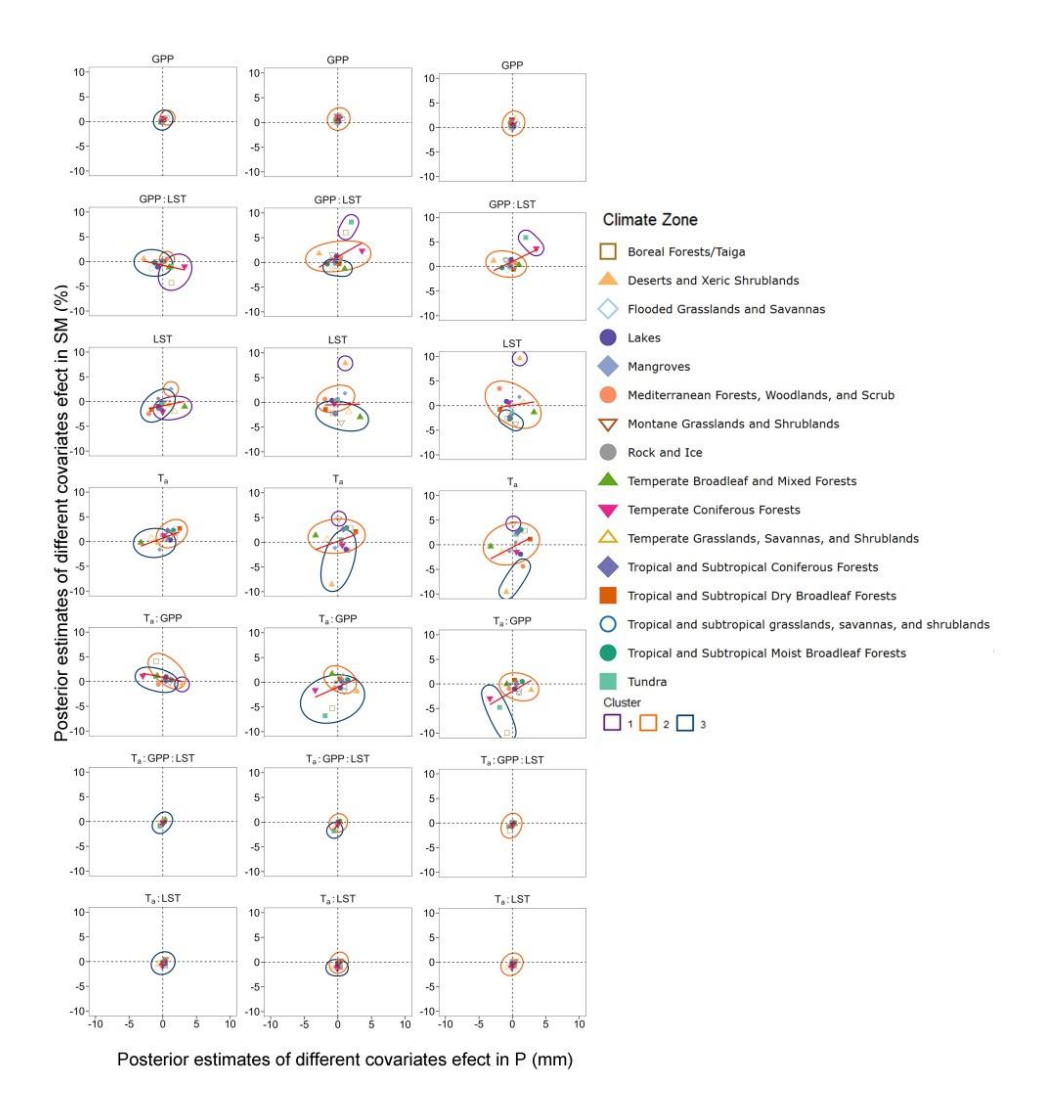


Fig. 7 Posterior estimates of the covariate variables of the Bayesian generalized non-linear multivariate multilevel model, built using monthly data. The columns represent soil depths of 0 to 7 cm, 7 to 28 cm, and 28 to 100 cm. Red lines indicate linear regressions of precipitation and soil moisture across all ecoregions, with cluster groups represented by three circles. The data point of each ecoregion belongs to a single and non-overlapping cluster.

The negative dependence in the surface layer across the Northern Hemisphere was primarily driven by the interactions between GPP:LST and Ta:GPP (Fig. 7). It shows that the regression trend line crosses quadrants II and IV. The negative relationship driven by GPP:LST was predominantly concentrated in quadrant IV, where increased precipitation lead to decreased soil moisture in the boreal forest, tundra, temperate coniferous forest, and temperate broadleaf mixed forest. The

negative dependence driven by Ta:GPP was mainly found in quadrant II, with distributions in deserts and xeric shrublands, boreal forests, montane grasslands and shrublands, temperate broadleaf mixed forests, and tundra. For the middle soil layer, GPP:LST drove a negative dependence in tropical and subtropical grasslands, savannas, shrublands, and tropical and subtropical coniferous forests. Ta and Ta:GPP drove in Mediterranean forests, woodlands, and scrub, as well as in temperate grasslands, savannas, and shrublands. The mixed effects of Ta:GPP:LST and Ta:LST had minimal impact across all ecological zones, with all estimates concentrated near the origin and only two clusters observed.

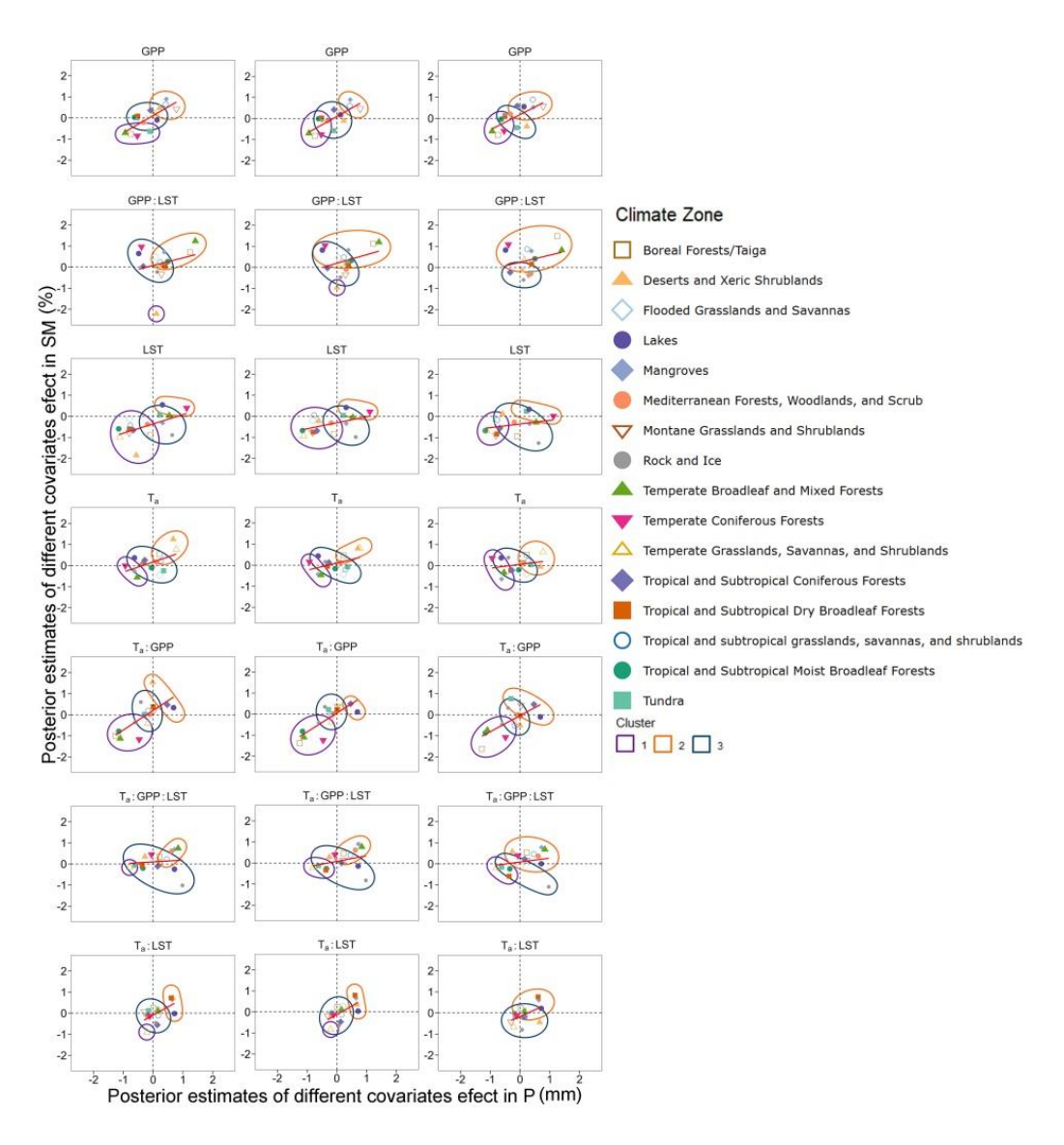


Fig. 8 Posterior estimates of the covariate variables of the Bayesian generalized non-linear multivariate multilevel model, built using annual data. The columns represent soil depths of 0 to 7 cm,

7 to 28 cm, and 28 to 100 cm. Red lines indicate linear regression of precipitation and soil moisture across all ecoregions, with cluster groups represented by three circles. The data point of each ecoregion belongs to a single and non-overlapping cluster.

472

473

474

475

476

477

478

479

480

481

482

483

484

485

486

487

488

489

490

491

492

493

494

495

469

470

471

Interannual negative dependence was primarily observed in the montane grasslands and shrublands region, where GPP:LST drove this pattern across all three soil layers. All other variables lead to positive dependence (Fig. 8). The long-term trend in the annual-scale Bayesian model revealed strong patterns, with the most significant difference compared to the monthly scale being the influence of T_a:GPP:LST and T_a:LST, where different ecological zones exhibited substantial variation. Among the multiple variables, T_a drove the most negative dependence, with the greatest differences observed between ecological zones. In the surface layer, LST alone drove the negative dependence in the mangrove, rock, and ice regions. Ta drove the negative dependence in tropical and subtropical coniferous forests, lakes, and rock and ice regions. In the middle soil layers, the negative dependence driven by T_a was in temperate forests, arid shrublands, and flooded grasslands and savannas, while it driven by Ta:GPP was in tropical and subtropical moist broadleaf forests. The negative dependence driven by Ta:LST was fully distributed in quadrant IV. This pattern was observed in regions such as the montane grasslands and shrublands, tropical and subtropical coniferous forests, tropical and subtropical grasslands, savannas, and shrublands; and rock and ice regions. The strongest drivers of negative dependence in the deep layers were GPP:LST and T_a. The negative dependence driven by GPP:LST was found in the rock and ice regions, Mediterranean forests, woodlands, and scrub, as well as tundra and temperate coniferous forests in quadrant II. The negative dependence driven by T_a was observed in rock and ice regions, lakes, and temperate coniferous forests in quadrant II, and flooded grasslands and savannas in quadrant IV.

4. Discussion

496

497

498

499

500

501

502

503

504

505

506

507

508

509

510

511

512

513

514

515

516

517

518

519

520

521

522

523

4.1 Characteristics of negative dependence areas

In this study, joint distributions of precipitation and soil moisture were constructed using Kendall's τ to characterize the nonlinear relationship. Consistent with previous findings, we observed a negative dependence between precipitation and soil moisture, particularly in arid and semi-arid regions (Qing et al., 2023; Yang et al., 2018). At the monthly scale, τ values in surface layer were stronger, indicating that seasonal dynamics—such as intermittent rainfall events followed by rapid soil moisture loss through evapotranspiration—likely drive the observed negative correlation. While negative dependence generally decreases with depth, the middle layer shows an unexpectedly low percentage. This layer often corresponds to the main root zone, where stable plant water uptake reduces soil moisture variability and weakens the feedback signal, leading to a few grid cells with significant negative dependence (Thompson et al., 2010). In contrast, the deep soil layers may retain some long-term memory of moisture deficits, especially under prolonged dry conditions, which could contribute to stronger negative dependence than in the more buffered middle layer. On the annual scale, the negative dependence may instead reflect longterm climate feedbacks. In high-latitude regions, for example, Arctic amplification and permafrost thawing can decouple precipitation inputs from effective soil moisture retention, leading to persistent moisture deficits despite increasing precipitation trends. Regions showing negative dependence between precipitation and soil moisture are primarily distributed in arid, semi-arid and cold high-latitude climates. Representative ecosystems include deserts and xeric shrublands, montane grasslands and shrublands, and Arctic tundra. Despite their climatic differences, these ecosystems share key ecohydrological traits, including limited precipitation input, strong evapotranspiration demand, sparse vegetation cover, and low soil moisture retention capacity.

Different from monthly scale, the negative dependence at annual scale is

primarily generated in regions such as deserts, xeric shrublands, montane grasslands and shrublands. These ecosystems are specifically characterized by arid conditions, and particularly sensitive to environmental changes, making them much responsive to long-term climatic variability. In deserts and xeric shrublands, annual precipitation typically falls below 250 mm, while evaporation consistently exceeds rainfall (Lockwood et al., 2006). Vegetation in these regions is dominated by shallow-rooted shrubs, which offer minimal resistance to post-rainfall moisture loss. As a result, soil moisture often declines rapidly following precipitation events, leading to a counterintuitive negative relationship between rainfall and moisture storage. Montane grasslands and shrublands, despite occurring in more topographically complex terrains, also experience dry climatic conditions characterized by low precipitation, high temperatures, and elevated VPD (Olson and Dinerstein, 1998). These factors enhance evapotranspiration, limiting the effectiveness of rainfall in replenishing soil moisture. Consequently, increases in precipitation may coincide with soil moisture decline due to enhanced moisture loss. In contrast, Arctic tundra ecosystems—such as those found in northern North America and Eurasia—are defined by cold temperatures, continuous permafrost, and moderate but ineffective precipitation. Frozen soils impede infiltration, causing much of the precipitation to be lost as surface runoff rather than retained in the soil profile. Dominant vegetation includes mosses, sedges, and dwarf shrubs with shallow root systems, further limiting water uptake and storage (Olson and Dinerstein, 1998; Xue et al., 2021).

524

525

526

527

528

529

530

531

532

533

534

535

536

537

538

539

540

541

542

543

544

545

546

547

548

549

550

551

- 4.2 Mechanism of negative dependence between precipitation and soil moisture
- 4.2.1 Energy-Driven Mechanism: LST and Ta-Driven ET Dominance

Negative dependence between precipitation and soil moisture was observed across several dry and cold ecoregions, including deserts and xeric shrublands, montane grasslands and shrublands, tundra. These regions are generally characterized by low precipitation and GPP, limiting vegetation's ability to retain or utilize moisture

effectively (Olson and Dinerstein, 1998; Xue and Wu, 2023). In arid ecosystems, shallow-rooted vegetation and high temperatures result in rapid soil moisture loss following rainfall. In montane environments, stronger warming trends (Pepin et al., 2022) and shallow-rooted vegetation (Stocker et al., 2023) further limit precipitation use, despite increased GPP under warming. Besides, the surface soil induced upward movement of soil water from the middle layer due to the osmotic and matric potential, further contributing to moisture depletion. In semi-arid grasslands, the interaction between soil texture and precipitation patterns further reinforces negative dependence. Brief rainfall events primarily moisten upper clay layers where grass roots concentrate (Sala and Lauenroth, 1985), while well-developed clay horizons restrict deep water percolation and shrub root expansion (Buxbaum and Vanderbilt, 2007). This physical confinement exacerbates water loss when increased GPP and LST enhance evapotranspiration from the shallow moistened zone, intensifying the precipitationsoil moisture decoupling. High temperatures can lead to surface soil sealing, preventing rainfall from effectively entering the root zone. Model simulations confirm that in flat arid regions (Koukoula et al., 2021), such soil barriers promote the "dry soil advantage"—where precipitation triggers runoff rather than infiltration.

552

553

554

555

556

557

558

559

560

561

562

563

564

565

566

567

568

569

570

571

572

573

574

575

576

577

578

579

580

The boreal forest and tundra ecosystems, often with permafrost, are temperature-limited systems. Precipitation often falls as snow, which accumulates on the surface. Then, a low LST can cause soil freezing, and the presence of surface withered litter may further insulate the soil, preventing timely moisture replenishment. Permafrost in these regions can lead to surface runoff of some precipitation, preventing effective infiltration into the soil. The geological conditions, such as Karst landforms can also influence the relationship between precipitation and soil moisture.

4.2.2 Biotic-Driven Mechanism: Vegetation Water Use and GPP Dominance

High-altitude ecosystems, especially in the Arctic and Qinghai–Tibetan Plateau, are increasingly affected by warming and variable precipitation (Lamprecht et al., 2018). These changes lead to reduced species abundance and increased GPP (Berauer et al., 2019). In montane grasslands and shrublands, species abundance negatively

correlates with soil nutrients and microbial functions (Graham Emily et al., 2024). Rising LST and extreme precipitation reduce microbial biomass and release soil minerals (Siebielec et al., 2020), intensifying light competition and lowering ecosystem stability. Biodiversity loss decreases soil water capacity, with some of these regions at high risk of water erosion (Straffelini et al., 2024).

Soil moisture reduction in the surface and middle layer is mainly driven by root water uptake under high LST and GPP. Roots shift absorption to deeper layers during droughts (Yadav Brijesh et al., 2009). In dry seasons, plants in grasslands and shrublands retain leaves to support evaporative cooling (Prior et al., 1997), this strategy also seen in deserts and xeric shrublands, where winter precipitation and freezing reduce surface moisture. Even during rainfall, soil moisture may decline due to evapotranspiration, runoff, and plant uptake (Tomlinson et al., 2013), creating a negative precipitation—soil moisture relationship. Canopy interception also limits infiltration (Zhong et al., 2022). However, in high-latitude ecosystems like boreal forests and tundra, warming mitigates cold limitations, allowing precipitation to increase soil moisture, shifting the relationship to positive.

Negative dependence in mid-to-deep soil layers can occur when a single factor dominates, limiting ecosystem compensation (Jarvis, 2011; Taylor and Klepper, 1979). In contrast, positive dependence may arise from synergistic interactions between GPP and LST. Higher GPP can reflect deeper root systems or improved water-use efficiency, while increased LST may enhance soil moisture release and promote water availability together (Wang et al., 2008). This interaction may strengthen ecosystem feedbacks—e.g., higher GPP can improve soil structure through biomass and organic matter, boosting water retention (Chen et al., 2025). Such synergy can offset LST-driven evapotranspiration and enhance ecosystem resilience, particularly through freeze—thaw processes in cold regions.

4.3 Data reliability

In this study, multiple observational datasets were employed to reduce modeldriven uncertainty and enhance data reliability. CRU TS, ESA CCI, and GPCP were selected due to their direct reliance on ground-based or satellite observations, in contrast to the model-based ERA5-Land product. Although ERA5 does offer a wide range of meteorological variables, it can introduce model uncertainties. Therefore, the datasets used in this study have independent source, which can avoid the potential false relationships between soil moisture and precipitation that may be caused by the same model architecture and input parameters. To investigate spatial heterogeneity, all data were spatially aggregated by ecoregion boundaries from the Conservation Biology Institute. These boundaries may introduce regional biases, which should be considered when interpreting the results.

The copula method can access the dependence between different time series, after removing influences of the conditional means and variances as well as marginal distributions (Durante et al., 2025; Neumeyer et al., 2019). In this study, although precipitation—soil moisture dependence was assessed across different time scales, the monthly series were not de-seasonalized. As a result, the residual seasonal signals may influence short-term dependence structures. This limitation will be addressed in future work through seasonal adjustment. In the Bayesian modeling, GPP, LST, and air temperature were examined as drivers of negative dependence. Evapotranspiration was excluded due to its dependence on both soil moisture and temperature. We acknowledge that additional factors—such as wind, topography, and soil physical properties—may also modulate precipitation—soil moisture coupling but were not in the scope of this analysis. Future research incorporating these variables would provide a more comprehensive understanding of the underlying mechanisms.

5. Conclusion

This study explored the dependence relationships between precipitation and soil moisture at depths of 0 to 7 cm, 7 to 28 cm, and 28 to 100 cm from 2000 to 2019, by examining the control effect of precipitation volume, precipitation frequency, and evapotranspiration on soil moisture. Bayesian models were used to analyze the driving factors in the dependence of soil moisture to precipitation in different ecoregions of the Northern Hemisphere. The results suggest that, the negative

dependence proportion reached 19.2%, 0.7%, and 2.3% at monthly scale, while it was 3.0%, 4.0%, and 8.6% at annual scale, respectively, for the three soil layers. Precipitation volume predominantly controlled soil moisture in the Boreal forest/taiga, temperate grasslands, savannas, and shrublands, while precipitation frequency primarily controlled soil moisture in the high-latitude regions of the Northern Hemisphere. The combined influence of evapotranspiration and precipitation exhibited clear seasonal patterns. Evapotranspiration was the dominant driver of soil moisture dynamics during the growing season, with a regression coefficient proportion greater than 75%. In contrast, precipitation volume played a more significant role in the surface and middle layer of non-growing season, with areas under strong univariate control accounting for over 40% of the total area. Additionally, the influence of precipitation frequency on soil moisture increased with latitude, the proportion of the regression coefficient averaging from 36.5% to 91.3%, highlighting a shift in controlling factors across climatic gradients.

In regions such as temperate grasslands, savannas, shrublands, deserts, xeric shrublands, and tundra, negative dependencies between precipitation and soil moisture, driven by LST and Ta:GPP interactions, were observed. These negative dependencies were mainly attributed to the seasonality of precipitation in arid and semi-arid areas and the freeze—thaw processes in the soil, which hinder effective moisture replenishment, especially during winter when soil freezing prevents rainwater infiltration. In the intermediate and deep soil layers, negative dependencies were primarily driven by single variables, whereas positive dependencies resulted from multivariate interactions, likely due to the lack of compensatory mechanisms when a single variable dominated, or the enhancement of ecosystem feedbacks when both GPP and LST interacted. Additionally, when the ecosystem is simultaneously driven by GPP and LST, greater resilience may be exhibited.

At the annual scale, the area of negative dependence increased with soil depth, with the most pronounced negative dependencies occurring in the montane grasslands and shrublands region. In this region, negative dependencies at all three soil depths

were driven by the GPP:LST interaction. A possible explanation is the long-term 668 variability in precipitation and temperature, which may have influenced 669 geomorphology, vegetation structure, and soil water retention capacity. 670 671 Data availability 672 The ERA5-Land soil moisture dataset (DOI: https://doi.org/10.1175/1525-673 7541(2001)002<0036:GPAODD>2.0.CO;2) was obtained from the Copernicus 674 Climate Data Store (accessed on 18 March 2024). The GPCP precipitation dataset 675 (DOI: https://doi.org/10.7289/V56971M6.) was obtained from the NOAA National 676 Centers for Environmental Information (accessed on 11 March 2024). The Gross 677 primary production dataset (https://doi.org/10.5194/essd-14-1063-2022) was obtained 678 from TU Wien Research Data Repository (accessed on 23 October 2023). The CRU 679 TS v4.07 air temperature dataset (https://doi.org/10.1038/s41597-020-0453-3) was 680 obtained from the Climatic Research Unit (accessed on 20 August 2023). The ESA 681 682 CCI Land Surface Temperature dataset (https://dx.doi.org/10.5285/a7e811fe11d34df5abac6f18c920bbeb) was obtained from 683 the Centre for Environmental Data Analysis (accessed on 27 August 2024). GLEAM 684 Evapotranspiration data (https://doi.org/10.5194/gmd-10-1903-2017) was obtained 685 from the GLEAM project (accessed on 19 March 2024). Terrestrial Ecoregions 686 dataset (https://doi.org/10.1641/0006-3568(2001)051[0933:TEOTWA]2.0.CO;2) was 687 obtained from the World Wildlife Fund (accessed on 5 September 2024). 688 689 **Author Contributions** 690 SX: Conceptualization, Data curation, Formal analysis, Methodology, Software, 691

694 695 Draft, Writing - Review & Editing.

692

693

696

Validation, Visualization, Writing - Original Draft, Writing - Review & Editing. GW:

Conceptualization, Funding acquisition, Investigation, Supervision, Writing - Original

Conflicts of Interest

The authors declare that they have no conflict of interest.

Financial Support

This study was funded by the National Key Research and Development Program of China (2022YFF0801302), the National Natural Science Foundation of China (41930970 and 42077421).

703

697

699

Reference

- Adler, R.F., G.J. Huffman, A. Chang, R. Ferraro, P.-P. Xie, J. Janowiak, B. Rudolf, U. Schneider, S. Curtis, D.
 Bolvin, A. Gruber, J. Susskind, P. Arkin, and E. Nelkin. 2003. The Version-2 Global Precipitation
 Climatology Project (GPCP) Monthly Precipitation Analysis (1979–Present). *Journal of Hydrometeorology*. 4:1147-1167.
- Berauer, B.J., P.A. Wilfahrt, M.A.S. Arfin-Khan, P. Eibes, A. Von Heßberg, J. Ingrisch, M. Schloter, M.A.
 Schuchardt, and A. Jentsch. 2019. Low resistance of montane and alpine grasslands to abrupt changes in temperature and precipitation regimes. *Arctic, Antarctic, and Alpine Research*.
 51:215-231.
- Browne, W.J., and D. Draper. 2006. A comparison of Bayesian and likelihood-based methods for fitting multilevel models. *Bayesian Analysis*. 1:473-514.
- Bürkner, P.-C. 2017. brms : An R Package for Bayesian Multilevel Models Using Stan. *Journal of Statistical Software*. 80.
- Buxbaum, C.A.Z., and K. Vanderbilt. 2007. Soil heterogeneity and the distribution of desert and steppe plant species across a desert-grassland ecotone. *Journal of Arid Environments*. 69:617-632.
- 720 Cammalleri, C., C. De Michele, and A. Toreti. 2024. Exploring the joint probability of precipitation and 721 soil moisture over Europe using copulas. *Hydrol. Earth Syst. Sci.* 28:103-115.
- 722 Chen, G., Q. Wang, and T. Chen. 2025. Dominant effect and threshold response of soil moisture on global vegetation greening in the 21st century. *CATENA*. 254:109008.
- Cook, B.I., G.B. Bonan, and S. Levis. 2006. Soil Moisture Feedbacks to Precipitation in Southern Africa.
 Journal of Climate. 19:4198-4206.
- Drager, A.J., L.D. Grant, and S.C. van den Heever. 2022. A Nonmonotonic Precipitation Response to
 Changes in Soil Moisture in the Presence of Vegetation. *Journal of Hydrometeorology*.
 23:1095-1111.
- Durante, F., S. Fuchs, and R. Pappada. 2025. Clustering of compound events based on multivariate comonotonicity. *Spatial Statistics*. 66:100881.
- Feldman, A.F., A.G. Konings, P. Gentine, M. Cattry, L. Wang, W.K. Smith, J.A. Biederman, A. Chatterjee,
 J. Joiner, and B. Poulter. 2024. Large global-scale vegetation sensitivity to daily rainfall variability. *Nature*. 636:380-384.
- Gerken, T., B.L. Ruddell, R. Yu, P.C. Stoy, and D.T. Drewry. 2019. Robust observations of land-toatmosphere feedbacks using the information flows of FLUXNET. *npj Climate and Atmospheric* Science. 2:37.
- Graham Emily, B., A. Garayburu-Caruso Vanessa, R. Wu, J. Zheng, R. McClure, and D. Jones Gerrad. 2024. Genomic fingerprints of the world's soil ecosystems. *mSystems*. 9:e01112-01123.
- Gu, C., Q. Tang, G. Zhu, J. Ma, C. Gu, K. Zhang, S. Sun, Q. Yu, and S. Niu. 2021. Discrepant responses between evapotranspiration- and transpiration-based ecosystem water use efficiency to interannual precipitation fluctuations. *Agricultural and Forest Meteorology*. 303:108385.
- Haghighi, E., D.J. Short Gianotti, R. Akbar, G.D. Salvucci, and D. Entekhabi. 2018. Soil and Atmospheric
 Controls on the Land Surface Energy Balance: A Generalized Framework for Distinguishing
 Moisture-Limited and Energy-Limited Evaporation Regimes. Water Resources Research.
 54:1831-1851.
- Harris, I., T.J. Osborn, P. Jones, and D. Lister. 2020. Version 4 of the CRU TS monthly high-resolution gridded multivariate climate dataset. *Scientific Data*. 7:109.

- He, L., J. Guo, W. Yang, Q. Jiang, L. Chen, and K. Tang. 2023. Multifaceted responses of vegetation to
 average and extreme climate change over global drylands. *Science of The Total Environment*.
 858:159942.
- Hollmann, R., C.J. Merchant, R. Saunders, C. Downy, M. Buchwitz, A. Cazenave, E. Chuvieco, P. Defourny, G. de Leeuw, R. Forsberg, T. Holzer-Popp, F. Paul, S. Sandven, S. Sathyendranath, M. van Roozendael, and W. Wagner. 2013. The ESA Climate Change Initiative: Satellite Data Records for Essential Climate Variables. *Bulletin of the American Meteorological Society*. 94:1541-1552.
- Huffman, G.J., and D.T. Bolvin. 2013. Version 1.2 GPCP one-degree daily precipitation data set documentation. *NASA Goddard Space Flight Center Rep*.
- Jarvis, N.J. 2011. Simple physics-based models of compensatory plant water uptake: concepts and ecohydrological consequences. *Hydrol. Earth Syst. Sci.* 15:3431-3446.
- Joaquín Muñoz-Sabater, E.D., Anna Agustí-Panareda, Clément Albergel, Gabriele Arduini, Gianpaolo Balsamo, Souhail Boussetta, Margarita Choulga, Shaun Harrigan, Hans Hersbach, Brecht Martens, Diego G. Miralles, María Piles, Nemesio J. Rodríguez-Fernández, Ervin Zsoter, Carlo Buontempo, and Jean-Noël Thépaut. 2021. ERA5-Land: a state-of-the-art global reanalysis dataset for land applications. *Earth Syst. Sci. Data*. 13:4349–4383.
- Knapp, A.K., C. Beier, D.D. Briske, A.T. Classen, Y. Luo, M. Reichstein, M.D. Smith, S.D. Smith, J.E. Bell,
 and P.A. Fay. 2008. Consequences of more extreme precipitation regimes for terrestrial
 ecosystems. *Bioscience*. 58:811-821.
- Koster, R.D., Z.C. Guo, R.Q. Yang, P.A. Dirmeyer, K. Mitchell, and M.J. Puma. 2009. On the Nature of Soil
 Moisture in Land Surface Models. *Journal of Climate*. 22:4322-4335.
- Koukoula, M., C.S. Schwartz, E.I. Nikolopoulos, and E.N. Anagnostou. 2021. Understanding the Impact
 of Soil Moisture on Precipitation Under Different Climate and Meteorological Conditions: A
 Numerical Sensitivity Study Over the CONUS. *Journal of Geophysical Research: Atmospheres*.
 126:e2021JD035096.
- Lamprecht, A., P.R. Semenchuk, K. Steinbauer, M. Winkler, and H. Pauli. 2018. Climate change leads to
 accelerated transformation of high elevation vegetation in the central Alps. New
 Phytologist. 220:447-459.
- 777 Li, W., M. Migliavacca, M. Forkel, J.M.C. Denissen, M. Reichstein, H. Yang, G. Duveiller, U. Weber, and 778 R. Orth. 2022. Widespread increasing vegetation sensitivity to soil moisture. *Nature* 779 *Communications*. 13.
- Lockwood, M., G. Worboys, and A. Kothari. 2006. Managing Protected Areas: A Global Guide. Farthscan, London, Sterling.
- Lv, P.F., H.F. Hao, and G.C. Wu. 2023. Differences in Global Precipitation Regimes between Land and Ocean Areas Based on the GPM IMERG Product. *Remote Sensing*. 15.
- 784 Ma, S., T. Zhou, A. Dai, and Z. Han. 2015. Observed Changes in the Distributions of Daily Precipitation 785 Frequency and Amount over China from 1960 to 2013. *Journal of Climate*. 28:6960-6978.
- Mao, Y., G. Wu, G. Xu, and K. Wang. 2022. Reduction in Precipitation Seasonality in China from 1960 to 2018. *Journal of Climate*. 35:227-248.
- McColl, K.A., S.H. Alemohammad, R. Akbar, A.G. Konings, S. Yueh, and D. Entekhabi. 2017. The global distribution and dynamics of surface soil moisture. *Nature Geoscience*. 10:100-+.
- 790 McDonald, G.C. 2009. Ridge regression. WIREs Computational Statistics. 1:93-100.
- 791 Miralles, D.G., T.R.H. Holmes, R.A.M. De Jeu, J.H. Gash, A.G.C.A. Meesters, and A.J. Dolman. 2011.

- 792 Global land-surface evaporation estimated from satellite-based observations. *Hydrol. Earth* 793 *Syst. Sci.* 15:453-469.
- Muñoz Sabater, J. 2019. ERA5-Land hourly data from 1950 to present. Copernicus Climate Change Service (C3S) Climate Data Store (CDS).
- 796 Myhre, G., K. Alterskjær, C.W. Stjern, Ø. Hodnebrog, L. Marelle, B.H. Samset, J. Sillmann, N. Schaller, E. 797 Fischer, M. Schulz, and A. Stohl. 2019. Frequency of extreme precipitation increases 798 extensively with event rareness under global warming. *Scientific Reports*. 9:16063.
- Nelsen, R.B. 2005. 14 Copulas and quasi-copulas: An introduction to their properties and applications. *In* Logical, Algebraic, Analytic and Probabilistic Aspects of Triangular Norms. E.P. Klement and R. Mesiar, editors. Elsevier Science B.V., Amsterdam. 391-413.
- Neumeyer, N., M. Omelka, and Š. Hudecová. 2019. A copula approach for dependence modeling in multivariate nonparametric time series. *Journal of Multivariate Analysis*. 171:139-162.
- Olson, D., and E. Dinerstein. 1998. The Global 200: A Representation Approach to Conserving the Earth's Most Biologically Valuable Ecoregions. *Conservation Biology*. 12:502-515.
- Olson, D.M., E. Dinerstein, E.D. Wikramanayake, N.D. Burgess, G.V.N. Powell, E.C. Underwood, J.A. D'Amico, I. Itoua, H.E. Strand, J.C. Morrison, C.J. Loucks, T.F. Allnutt, T.H. Ricketts, Y. Kura, J.F. Lamoreux, W.W. Wettengel, P. Hedao, and K.R. Kassem. 2001. Terrestrial Ecoregions of the World: A New Map of Life on Earth: A new global map of terrestrial ecoregions provides an innovative tool for conserving biodiversity. *BioScience*. 51:933-938.
- Pepin, N.C., E. Arnone, A. Gobiet, K. Haslinger, S. Kotlarski, C. Notarnicola, E. Palazzi, P. Seibert, S. Serafin, W. Schöner, S. Terzago, J.M. Thornton, M. Vuille, and C. Adler. 2022. Climate Changes and Their Elevational Patterns in the Mountains of the World. *Reviews of Geophysics*. 60:e2020RG000730.

815

816

817

- Prior, L.D., D. Eamus, and G.A. Duff. 1997. Seasonal and Diurnal Patterns of Carbon Assimilation, Stomatal Conductance and Leaf Water Potential in <emph type="2">Eucalyptus tetrodonta</emph> Saplings in a Wet–Dry Savanna in Northern Australia. Australian Journal of Botany. 45:241-258.
- Qiao, L., Z. Zuo, R. Zhang, S. Piao, D. Xiao, and K. Zhang. 2023. Soil moisture-atmosphere coupling accelerates global warming. *Nature communications*. 14:4908-4908.
- Qing, Y., S. Wang, Z.-L. Yang, and P. Gentine. 2023. Soil moisture—atmosphere feedbacks have triggered the shifts from drought to pluvial conditions since 1980. *Communications Earth & Environment*. 4:254.
- Sala, O.E., and W.K. Lauenroth. 1985. Root Profiles and the Ecological Effect of Light Rainshowers in Arid and Semiarid Regions. *The American Midland Naturalist*. 114:406-408.
- Sehler, R., J. Li, J.T. Reager, and H. Ye. 2019. Investigating Relationship Between Soil Moisture and Precipitation Globally Using Remote Sensing Observations. *Journal of Contemporary Water Research & Education*. 168:106-118.
- shen, S., S. Ye, C. Cheng, C. Song, J. Gao, J. Yang, L. Ning, K. Su, and T. Zhang. 2018. Persistence and Corresponding Time Scales of Soil Moisture Dynamics During Summer in the Babao River Basin, Northwest China. *Journal of Geophysical Research: Atmospheres*. 123:8936-8948.
- Shen, Z., M. Hua, J. Lu, C. Zhang, and J. Fang. 2016. Response of soil moisture to precipitation in the valley mountain Lhasa, Tibet. *China Rural. Water Hydropower*. 10:104-107.
- Siebielec, S., G. Siebielec, A. Klimkowicz-Pawlas, A. Gałązka, J. Grządziel, and T. Stuczyński. 2020.

 Impact of water stress on microbial community and activity in sandy and loamy soils.

- 836 *Agronomy*. 10:1429.
- Stocker, B.D., S.J. Tumber-Dávila, A.G. Konings, M.C. Anderson, C. Hain, and R.B. Jackson. 2023. Global patterns of water storage in the rooting zones of vegetation. *Nature Geoscience*. 16:250-256.
- Straffelini, E., J. Luo, and P. Tarolli. 2024. Climate change is threatening mountain grasslands and their cultural ecosystem services. *CATENA*. 237:107802.
- Szutu, D.J., and S.A. Papuga. 2019. Year-Round Transpiration Dynamics Linked With Deep Soil Moisture in a Warm Desert Shrubland. *Water Resources Research*. 55:5679-5695.
- Taylor, C.M., R.A.M. de Jeu, F. Guichard, P.P. Harris, and W.A. Dorigo. 2012. Afternoon rain more likely over drier soils. *Nature*. 489:423-426.
- Taylor, H.M., and B. Klepper. 1979. The Role of Rooting Characteristics in the Supply of Water to Plants11Journal Paper J-8906 of the Iowa Agriculture and Home Economics Experiment Station, Ames, Iowa, Project No. 1941, and Technical Paper 4673 of the Oregon State University Agricultural Experiment Station, Pendleton, Oregon. *In* Advances in Agronomy. Vol. 30. N.C. Brady, editor. Academic Press. 99-128.
- Thompson, S.E., C.J. Harman, P. Heine, and G.G. Katul. 2010. Vegetation-infiltration relationships across climatic and soil type gradients. *Journal of Geophysical Research: Biogeosciences*. 115.
- Tomlinson, K.W., L. Poorter, F.J. Sterck, F. Borghetti, D. Ward, S. de Bie, and F. van Langevelde. 2013.

 Leaf adaptations of evergreen and deciduous trees of semi-arid and humid savannas on three continents. *Journal of Ecology*. 101:430-440.
- Vereecken, H., J.A. Huisman, H. Bogena, J. Vanderborght, J.A. Vrugt, and J.W. Hopmans. 2008. On the value of soil moisture measurements in vadose zone hydrology: A review. *Water Resources Research*. 44.
- Vidana Gamage, D.N., A. Biswas, and I.B. Strachan. 2020. Scale and location dependent time stability of soil water storage in a maize cropped field. *CATENA*. 188:104420.
- Wang, G., Y. Li, H. Hu, and Y. Wang. 2008. Synergistic effect of vegetation and air temperature changes
 on soil water content in alpine frost meadow soil in the permafrost region of Qinghai-Tibet.
 Hydrological Processes. 22:3310-3320.
- Wang, J., D. Liu, P. Ciais, and J. Penuelas. 2022. Decreasing rainfall frequency contributes to earlier leaf onset in northern ecosystems. *Nature Climate Change*. 12:386-+.
- Wild, B., I. Teubner, L. Moesinger, R.M. Zotta, M. Forkel, R. van der Schalie, S. Sitch, and W. Dorigo.
 2022. VODCA2GPP a new, global, long-term (1988–2020) gross primary production dataset
 from microwave remote sensing. *Earth Syst. Sci. Data*. 14:1063-1085.
- Wu, G., Y. Li, S. Qin, Y. Mao, and K. Wang. 2021. Precipitation unevenness in gauge observations and eight reanalyses from 1979 to 2018 over China. *Journal of Climate*. 34:9797–9810.
- Wullschleger, S., and P. Hanson. 2006. Sensitivity of canopy transpiration to altered precipitation in an upland oak forest: evidence from a long-term field manipulation study. *Global Change Biology*. 12:97-109.
- Xiao, T., P. Li, W. Fei, and J. Wang. 2024. Effects of vegetation roots on the structure and hydraulic properties of soils: A perspective review. *Science of The Total Environment*. 906:167524.
- Xue, S., and G. Wu. 2023. Sensitivities of Vegetation Gross Primary Production to Precipitation Frequency in the Northern Hemisphere from 1982 to 2015. *Remote Sensing*. 16:21.
- Xue, S., and G. Wu. 2024. Causal inference of root zone soil moisture performance in drought.

 Agricultural Water Management. 305:109123.
- Xue, S.-Y., H.-Y. Xu, C.-C. Mu, T.-H. Wu, W.-P. Li, W.-X. Zhang, I. Streletskaya, V. Grebenets, S. Sokratov,

880 A. Kizyakov, and X.-D. Wu. 2021. Changes in different land cover areas and NDVI values in 881 northern latitudes from 1982 to 2015. Advances in Climate Change Research. 12:456-465. Yadav Brijesh, K., S. Mathur, and A. Siebel Maarten. 2009. Soil Moisture Dynamics Modeling 882 883 Considering the Root Compensation Mechanism for Water Uptake by Plants. Journal of 884 Hydrologic Engineering. 14:913-922. 885 Yang, L., G. Sun, L. Zhi, and J. Zhao. 2018. Negative soil moisture-precipitation feedback in dry and wet 886 regions. Scientific Reports. 8:4026. 887 Zhang, P., P. Xiao, W. Yao, G. Liu, and W. Sun. 2020. Profile distribution of soil moisture response to 888 precipitation on the Pisha sandstone hillslopes of China. Scientific Reports. 10:9136. 889 Zhang, W., T. Zhou, and P. Wu. 2024. Anthropogenic amplification of precipitation variability over the 890 past century. Science. 385:427-432. 891 Zhong, F., S. Jiang, A.I.J.M. van Dijk, L. Ren, J. Schellekens, and D.G. Miralles. 2022. Revisiting large-892 scale interception patterns constrained by a synthesis of global experimental data. Hydrol. 893 Earth Syst. Sci. 26:5647-5667. 894 Zhou, S., A.P. Williams, B.R. Lintner, A.M. Berg, Y. Zhang, T.F. Keenan, B.I. Cook, S. Hagemann, S.I. Seneviratne, and P. Gentine. 2021. Soil moisture-atmosphere feedbacks mitigate declining 895 896 water availability in drylands. Nature Climate Change. 11:274-274. 897 Zhu, Q., X. Nie, X. Zhou, K. Liao, and H. Li. 2014. Soil moisture response to rainfall at different 898 topographic positions along a mixed land-use hillslope. Catena. 119:61-70.